Blind sequence-length estimation of low-SNR cyclostationary sequences

J.D. Vlok and J.C. Olivier

***Abstract*—Several existing direct-sequence spread spectrum (DSSS) detection and estimation algorithms assume prior knowledge of the symbol period or sequence length, although very few sequence-length estimation techniques are available in the literature. This paper presents two techniques to estimate the sequence length of a baseband DSSS signal affected by additive white Gaussian noise (AWGN). The first technique is based on a known autocorrelation technique which is used as reference, and the second technique is based on principal component analysis (PCA). Theoretical analysis and computer simulation show that the second technique can correctly estimate the sequence length at a lower signal-to-noise ratio (SNR) than the first technique. The techniques presented in this paper can estimate the sequence length blindly which can then be fed to semi-blind detection and estimation algorithms.**

I. Introduction

In non-cooperative reception, blind detection and estimation techniques are required as the parameters used by the communication transmitter are in general not known by the receiver. The normal approach used in cooperative communication systems, such as optimal correlation or matched filtering techniques [1], is therefore not applicable in non-cooperative communication receiver systems. Typical applications of such systems are to be found in spectrum surveillance and electronic interception, but blind estimation techniques are important in their own right also [2], and hence this paper considers some aspects of this problem in depth.

Signal detection and parameter estimation are usually performed separately and independently in communication problems [3]. Detection is performed to determine whether the signal of interest is present or absent given observed data that is corrupted by noise. When it has been determined that the signal of interest is present, estimation is performed to determine the signal parameter values. This paper is concerned with blind estimation (assuming the signal is present) of the period of cyclostationary sequences used in direct-sequence spread spectrum (DSSS) communication systems.

The spreading codes used in DSSS are cyclostationary, since the mean and autocorrelation of the transmitted signal are periodic with the same period [4]. This periodicity distinguishes the signal from noise and can be exploited to perform detection and estimation especially when the signals are weak. This is in fact the case for received DSSS, especially for a non-cooperative receiver which does not know the spreading code and cannot therefore take advantage of the processing gain. Furthermore, modern communication systems use feedback to limit transmit power levels. The resultant effect is that intercepted DSSS signals have very low signal-to-noise ratio (SNR) levels and sophisticated algorithms are required to perform detection and estimation reliably.

We wish to emphasise that blind estimation of the sequence or code length (or symbol period) of hidden DSSS transmissions is essential since semi-blind techniques often assume knowledge of the sequence length which is generally not known *a priory*. Such semi-blind techniques include sequence estimation techniques [5]–[7] and detection algorithms [8].

A few techniques that may be used to estimate the sequence length (or related parameters from which the sequence length can be determined) of DSSS transmissions have been suggested in the literature. These include cyclic-feature analysis to determine the chip rate through spectral-line regeneration [9], the related Fourier analysis of cyclic correlation to estimate the bit rate [6], and higher-order statistical analysis where unique bispectrum and triple correlation patterns reveal characteristics of m-sequences that may be used to determine the sequence length and generator polynomials [10]. These techniques however require relatively high SNRs to perform parameter estimation. Another technique based on autocorrelation suggested in [11], [12] has the potential to estimate the sequence length at lower SNR values.

In this paper, we propose two new methods to estimate the sequence length of an intercepted DSSS signal at low SNR, and we present some novel results based on these new methods. The first method is based on the autocorrelation technique [11], [12] mentioned above, and the second method on a principal component analysis (PCA) detection technique [8]. The two techniques are compared in an additive white Gaussian noise (AWGN) environment in terms of the probability of correct estimation of the sequence length.

The paper is organised as follows. Section II presents the communication and intercept systems, and defines the SNR regime to which the estimation is applied. The two new methods are introduced in Sections III and IV. Section V presents numerical results, and Section VI concludes the paper. Possible future research areas are identified in Section VII. A Barker code (length $N = 11$) and an m-sequence ($N = 63$) are considered as test cases throughout the paper.

II. Communication and intercept systems

The target communication system and intercept receiver platform used in this study are identical to those used in our previous study [8] and are briefly reviewed here.

The target communication system is a binary phase shift keying (BPSK) DSSS system employing a length-N spreading

J.D. Vlok is with Defence, Peace, Safety & Security (DPSS), Council for Scientific and Industrial Research (CSIR), Pretoria, South Africa, 0001. E-mail: jvlok@csir.co.za

J.C. Olivier is with the School of Engineering, University of Tasmania, Hobart, Australia, 7005.

code, such that the intercepted signal can be written as

$$\boldsymbol{y}(nT_c) = \sigma_x \boldsymbol{d}(nT_c)\boldsymbol{c}(nT_c) + \sigma_w \boldsymbol{w}(nT_c) \tag{1}$$

with the chip number $n = 1, 2, \ldots, N$ and T_c the chip interval. One sample is used to represent a single chip in the intercept receiver and therefore the sampling period $T_s = T_c$. $\boldsymbol{c}$ is the length-N ($N \gg 1$) pseudo-noise code sequence with period $T_{sym} = NT_c$ and $\boldsymbol{d}$ the data sequence assumed to be invariant over T_{sym}. Since the target communication system is a BPSK DSSS system, both $\boldsymbol{c}$ and $\boldsymbol{d}$ are sequences with values ± 1. The noise sequence is assumed to be a realisation of a standard normal random variable (RV) represented by $\boldsymbol{w} \sim \mathcal{N}(0, 1)$ which contains independent and identically distributed (i.i.d.) samples. The code, data and noise sequences are also assumed independent of each other. The constants σ_x and σ_w are included to scale the signal and noise sequences respectively in order to obtain different SNR values, using

$$\text{SNR} = \frac{\sigma_x^2}{\sigma_w^2} \tag{2}$$

which is the SNR before despreading. The SNR at which the intercept receiver must be able to operate is dictated by the SNR required by the intended or target DSSS communication receiver system, which in turn is determined by the maximum tolerable bit error rate (BER). The error probability or BER and the SNR are related by [8]

$$P_e = Q\left(\sqrt{N_s \ \text{SNR}}\right) \tag{3}$$

with N_s the number of samples used to represent one transmitted bit. If one spreading sequence chip is represented by one sample in the receiver, then $N_s = N$. Fig. 1 shows the BER curves for the unspreaded BPSK case ($N = 1$) and two spreaded cases ($N = 11$ and $N = 63$) under AWGN conditions. Spreading affords a processing gain $P_G = 10 \log_{10} N$ or SNR advantage to the intended DSSS receiver over the intercept receiver. For example, the receiver of a DSSS communication system using $N = 63$ ($P_G \approx 18$ dB) can despread a received signal at SNR = -3 dB to SNR = 15 dB to achieve $P_e \approx 10^{-8}$. An intercept receiver that does not know the spreading code will have to deal with the SNR = -3 dB signal, assuming the intended and intercept receivers lie on a circle with the target transmitter in the centre with an omnidirectional antenna. Identical channel conditions between the transmitter and each receiver are also assumed. If the transmitter uses a directional antenna and/or the intercept receiver is located at a further distance (which is typical in electronic interception scenarios), an even lower SNR will result.

To compete with the target DSSS communication system, the intercept receiver must be equipped with powerful techniques to detect the signals and estimate their parameter values at very low SNR levels. The BER that can be tolerated in a system depends on the application; it has been reported that in wireless multimedia transmission, voice packets can tolerate maximum BER levels of 10^{-3}, while data packets require a BER less than 10^{-9} [13]. Using Fig. 1, these BER values translate to minimum SNR levels of approximately -8.2 dB (-0.6 dB) for voice and -2.4 dB (5.1 dB) for data if $N = 63$ ($N = 11$) is used. The lower the SNR value at which a detection or estimation technique can function, the larger the detection range or intercept distance will be. In electronic intercept applications, SNR values less than the values given above will typically be required.

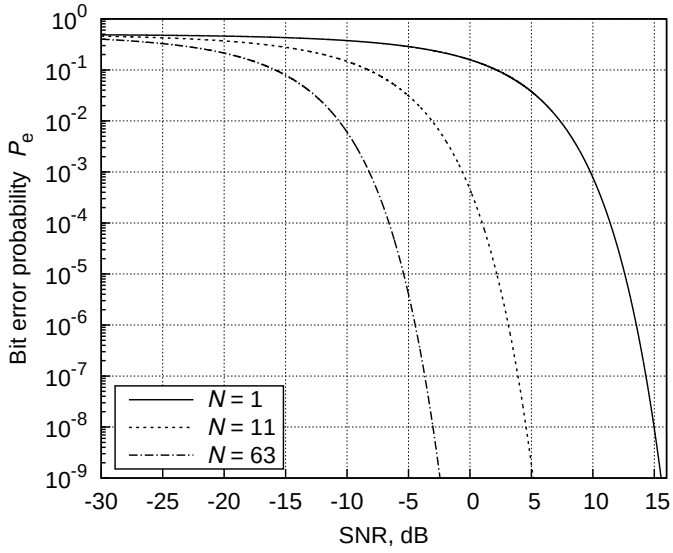

Fig. 1. Bit error probability for unspreaded ($N = 1$) and spreaded ($N = 11$ and $N = 63$) BPSK DSSS in AWGN

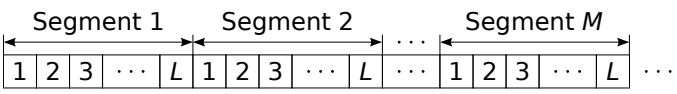

Fig. 2. Segmented section of the intercepted signal consisting of ML samples

III. Estimation technique 1: Autocorrelation

It has been suggested that the time interval between autocorrelation spikes of an intercepted DSSS signal can be used to estimate the symbol period T_{sym} [11]. However, this section proposes a new estimation technique with detailed mathematical analysis, which is based on the concept that the correlation can be performed such that the index value of the first peak corresponds to the sequence length.

A. Mean-square correlation

The intercepted signal of (1) can be expressed as

$$\boldsymbol{y} = \sigma_x d\boldsymbol{c} + \sigma_w \boldsymbol{w} \tag{4}$$

with the data bit value $d = \pm 1$ constant over a single spreading code. The first ML samples of $\boldsymbol{y}$ are split into M segments, such that each segment contains L samples as shown in Fig. 2.

A sliding correlation is then calculated between the m^{th} ($m = 1, 2, \ldots, M$) segment and the neighbouring section to the right within $\boldsymbol{y}$ using

$$R_{yy}^{(m)}(k) = \frac{1}{\sqrt{L}} \sum_{n=1}^{L} y_n \ y_{n+k} \tag{5}$$

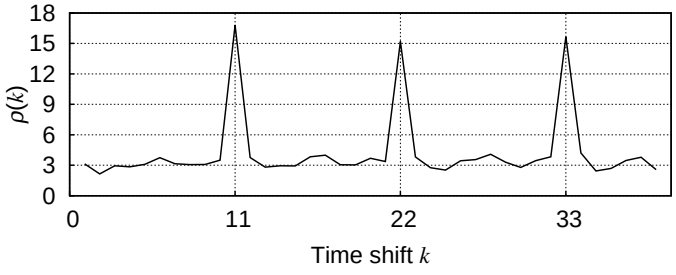

(a) $K = 39$ and SNR = 0 dB

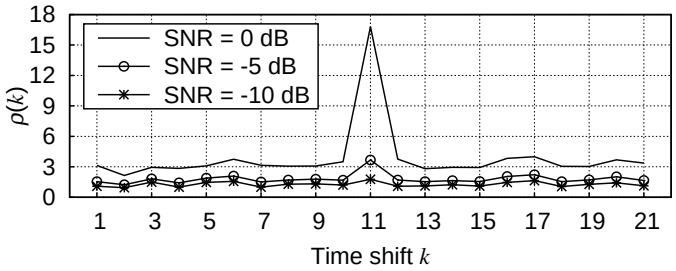

(b) $K = 21$ and SNR = $\{-10, -5, 0\}$ dB

Fig. 3. Simulated mean-square correlation sequences for $L = N = 11$ and $M = 100$ for the Barker-11 code

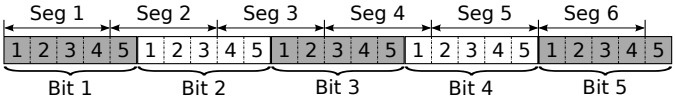

(a) $L < N$, which will produce partial correlation results

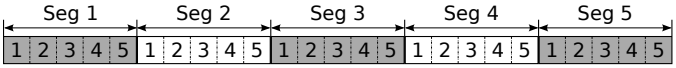

(b) $L = N$ (ideal case) where segments and sequences are aligned

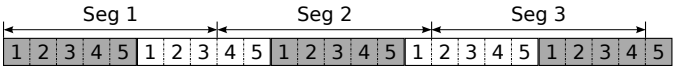

(c) Case where $N < L < 2N - 1$

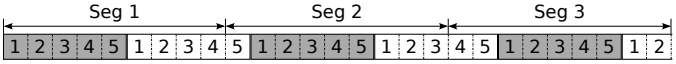

(d) Case where $L = 2N - 1$

Fig. 4. Example of a length $N = 5$ spreading sequence to illustrate the effect of the segment length L on the correlation process

with the time-shift parameter $k = 1, 2, \ldots, K$ and the scale factor $\sqrt{L}$ chosen to simplify the mathematical analysis presented in Section III-C. The samples of $\boldsymbol{y}$ in (5) are numbered such that y_n is the n^{th} sample of the m^{th} segment in each case. For example, when calculating $R_{yy}^{(1)}(k)$, sample y_{L+2} will refer to sample 2 of segment 2 in Fig. 2. However, when calculating $R_{yy}^{(2)}(k)$ this same sample will be referred to as y_2. The scalar product of a segment with itself is not needed and therefore $k = 0$ is excluded from (5). K is the value of the maximum time shift and determines the number of samples required beyond the segmented ML samples.

Using the M correlation sequences defined by (5), the mean-square correlation sequence can be calculated as

$$\rho(k) = \frac{1}{M} \sum_{m=1}^{M} \left[R_{yy}^{(m)}(k) \right]^2 \tag{6}$$

which is similar to the correlation estimators of [11]. An example mean-square correlation sequence for the Barker $N = 11$ spreading code is shown in Fig. 3(a) with parameters $K = 39$, $L = 11$, $M = 100$ and $\sigma_x^2 = \sigma_w^2 = 1$ such that the SNR is 0 dB.

The number of correlation spikes (or peaks) depends on the maximum time-shift parameter K, while the visibility of the peaks within the noise (or correlation sidelobe values) depends on the segment length L, number of segments M, the position of spreading sequences within segments, and the SNR. Assuming the spikes are detectable, there will be at least one in $\rho(k)$ if $K \geq N$, two if $K \geq 2N$, three if $K \geq 3N$, and so on. Fig. 3(a) shows three clear spikes since $K \geq 3N$ and the SNR of 0 dB is relatively high. For increasing values of M and SNR, the peak values generally become more visible as long as L is chosen correctly and a complete spreading code is located within a segment. Fig. 3(a) was obtained by choosing the actual spreading sequences as segments, which is the ideal case for which the correlation peaks will be maximum.

Due to partial correlation, the sum in (5) will produce smaller correlation peaks if $L < N$. Similarly, for $L > N$ partial correlation caused by incomplete spreading codes within each segment will add to or subtract from the correlation between complete spreading codes, depending on the data bit values. Also, if $L \neq N$ the spreading codes and segments are misaligned, such that the starting positions of each spreading code will differ in neighbouring segments. Even if $L > N$, some segments might not contain a single complete sequence and smaller correlation peaks than possible with $L = N$ will be formed. To ensure that a segment will always contain at least one complete spreading code, either $L = N$ (with sequences and segments aligned) or $L \geq 2N - 1$.

To illustrate the effects of the value of L and the alignment between segments and spreading sequences on the correlation process, an example is shown in Fig. 4. The sequence length $N = 5$, and the first sample of the first segment is also the starting position of a spreading code in each of the four cases shown. Each bit is represented by 5 samples (chips) and has a unique value (± 1) independent of the other bit values.

The case where $L < N$ is shown in Fig. 4(a) where the segments and sequences are misaligned. Using (5) will therefore result in partial correlation - and smaller peak values. The ideal case is shown in Fig. 4(b), where $L = N$ and the alignment is retained throughout the intercepted signal. When (5) is applied to this scenario, two complete spreading sequences will be correlated, producing a large peak for each value of m. The case where $N < L < 2N - 1$ is shown in Fig. 4(c). The first two segments each contains a complete sequence, which will provide a peak value when (5) is calculated. The incomplete sequences within these two segments will however affect this peak value depending on the bit values. Segment 3 in Fig. 4(c) does not contain a complete sequence which will negatively affect the correlation process. When $L \geq 2N - 1$ as illustrated in Fig. 4(d), all segments will however contain at least one complete spreading sequence. The incomplete

sequences within each segment will also negatively affect the correlation peaks for this scenario, and the result will be worse compared with $L = N$ as in Fig. 4(b).

B. Method of estimation

Fig. 3(a) illustrates that if the parameters are chosen correctly and the SNR is sufficiently high, all correlation peaks will be located at index values k, which are equal to multiples of the code length N. For time shifts $k = aN$, with a a positive integer, the spreading code(s) within the m^{th} segment will align with spreading code(s) in $\boldsymbol{y}$, irrespective of the starting position of the spreading code(s) within the segment or $\boldsymbol{y}$. The correlation peak values will however depend on the alignment between segments and sequences as discussed in Section III-A above. The code length may therefore be determined from the index values of peaks within $\rho(k)$. In this paper we propose to use the index of the first peak ($a = 1$) to determine N.

C. Mathematical analysis

The intercepted signal of (4) can be written in discrete form as

$$y_n = \sigma_x d_i c_n + \sigma_w w_n \tag{7}$$

with $d_i = \pm 1$ the i^{th} data bit value and c_n the n^{th} ($n = 1, 2, \ldots, N$) chip of the spreading code. The ideal case corresponding to Fig. 4(b) will be analysed here and compared with simulation results of non-ideal cases in Section V. The segment size will therefore be chosen as $L = N$, such that each segment in Fig. 2 will contain one complete spreading code. Furthermore, the maximum time shift is assumed to be bounded according to $N \leq K \leq 2N - 1$, such that a single correlation peak is produced. Fig. 3(b) shows the resultant mean-square correlation sequence $\rho(k)$ for $K = 2N - 1$ and SNR = $\{-10, -5, 0\}$ dB with $\sigma_w^2 = 1$. A clear peak value is shown at $k = N$ if the SNR is sufficiently high.

1) Signal-only analysis: This section will consider the characteristics of $R_{yy}^{(m)}(k)$ and $\rho(k)$ defined respectively in (5) and (6), using (7) with $\sigma_w = 0$.

a) Peak value:

When $k = N$, the spreading codes within each segment align, such that (5) can be written using (7) as

$$\begin{aligned} R_{yy}^{(m)}(N) &= \frac{1}{\sqrt{L}} \sum_{n=1}^{L} y_n \; y_{n+N} \\ &= \frac{1}{\sqrt{L}} \sum_{n=1}^{L} \left(\sigma_x d_m c_n\right) \left(\sigma_x d_{m+1} c_{n+N}\right) \end{aligned} \tag{8}$$

where $d_m = \pm 1$ represents the data bit value associated with the m^{th} segment. Since $c_n = c_{n+N} = \pm 1$, (8) can be simplified as

$$R_{yy}^{(m)}(N) = \pm \sigma_x^2 \sqrt{L} \tag{9}$$

The mean-square correlation peak value can then be expressed using (6) as

$$\rho(N) = \sigma_x^4 L \tag{10}$$

b) Sidelobe values:

When $k \neq N$, the correlation between misaligned spreading codes can be expressed using (5) and (7) as

$$R_{yy}^{(m)}(k) = \frac{\sigma_x^2}{\sqrt{L}} \sum_{n=1}^{L} \left(d_p c_n\right) \left(d_q c_{n+k}\right) \tag{11}$$

with d_p and d_q antipodal bit values depending on the segment in which c_n and c_{n+k} are respectively located. The correlation values produced by (11) depend on the specific spreading code $\boldsymbol{c}$ and the data bit values. If $d_p = d_q$, (11) resembles the periodic autocorrelation function, for which a number of bounds have been derived [14], which can be used to evaluate the sidelobe levels.

Barker codes and maximum-length or m-sequences are of particular interest, since the unscaled periodic autocorrelation for each time shift ($k \neq N$) is ± 1. Even when $d_p \neq d_q$, the sum in (11) equals ± 1 if $\boldsymbol{c}$ is a Barker code of length $N = [5, 7, 11, 13]$. In these conditions, (11) can be simplified to

$$R_{yy}^{(m)}(k) = \pm \frac{\sigma_x^2}{\sqrt{L}} \tag{12}$$

such that the mean-square value can be written by substituting (12) into (6) as

$$\rho(k) = \frac{\sigma_x^4}{L} \tag{13}$$

Equation (12) will subsequently be used to derive the theoretical performance bound of technique 1.

2) Noise-only analysis: When $\sigma_x = 0$, the correlation sequence can be written by combining (5) and (7) as

$$R_{ww}^{(m)}(k) = \frac{\sigma_w^2}{\sqrt{L}} \sum_{n=1}^{L} w_n w_{n+k} \tag{14}$$

Since $w_n \sim \mathcal{N}(0, 1)$ is a sample within a sequence of i.i.d. samples, w_n and w_{n+k} will be independent when $k \neq 0$. The product $w_n w_{n+k}$ will therefore have a normal product distribution [15] with zero mean and unity variance. According to the central limit theorem [16], the sum in (14) will approach the normal distribution with zero mean and variance approaching L, as L increases. $R_{ww}^{(m)}(k)$ will therefore approach the normal distribution with zero mean and variance

$$\begin{aligned} \text{var}\left(R_{ww}\right) &= \left(\frac{\sigma_w^2}{\sqrt{L}}\right)^2 L \\ &= \sigma_w^4 \end{aligned} \tag{15}$$

The distribution of the mean-square correlation $\rho(k)$ can then be obtained by combining (6), (14) and (15) as

$$\begin{aligned} \rho(k) &= \frac{1}{M} \sum_{m=1}^{M} \left[R_{ww}^{(m)}(k)\right]^2 \\ &= \frac{1}{M} \sum_{m=1}^{M} \left[\sigma_w^2 \tilde{R}_{ww}^{(m)}(k)\right]^2 \\ &= \frac{\sigma_w^4}{M} \sum_{m=1}^{M} \left[\tilde{R}_{ww}^{(m)}(k)\right]^2 \end{aligned} \tag{16}$$

with $\tilde{R}_{ww}^{(m)}(k)$ normalised such that it has unity variance. The mean-square correlation can then be written from (16) as

$$\frac{M}{\sigma_w^4}\rho(k) = \sum_{m=1}^{M}\left[\tilde{R}_{ww}^{(m)}(k)\right]^2 \tag{17}$$

which has a central Chi-squared distribution [17] with M degrees of freedom. Note that, although $\tilde{R}_{ww}^{(m)}(k)$ contains correlated samples over k for any given value of m, the sum in (17) is calculated over m (and not over k) such that the summands are independent.

It can be confirmed in simulation that (14) and (17) approach, respectively, a normal distribution (with variance given by (15)) and a central Chi-squared distribution (with M degrees of freedom) as L increases.

3) Signal-and-noise analysis: When a signal is present within the noise, the correlation can be expressed by combining (5) and (7) as

$$\begin{aligned} R_{yy}^{(m)}(k) = \frac{1}{\sqrt{L}}\sum_{n=1}^{L}\{&(\sigma_x d_p c_n + \sigma_w w_n) \\ &\times (\sigma_x d_q c_{n+k} + \sigma_w w_{n+k})\} \end{aligned} \tag{18}$$

with d_p and d_q bit values depending on the value of k as in (11). Equation (18) can further be developed as

$$\begin{aligned} R_{yy}^{(m)}(k) = &\frac{\sigma_x^2}{\sqrt{L}}\sum_{n=1}^{L} d_p d_q c_n c_{n+k} \\ &+ \frac{\sigma_x\sigma_w}{\sqrt{L}}\sum_{n=1}^{L} d_p c_n w_{n+k} \\ &+ \frac{\sigma_x\sigma_w}{\sqrt{L}}\sum_{n=1}^{L} d_q c_{n+k} w_n \\ &+ \frac{\sigma_w^2}{\sqrt{L}}\sum_{n=1}^{L} w_n w_{n+k} \end{aligned} \tag{19}$$

The first term of (19) is non-random while the remaining terms are random since they contain the noise sample $w \sim \mathcal{N}(0,1)$. The second and third terms of (19) are both normally distributed with zero mean and variance

$$\sigma^2 = \sigma_x^2\sigma_w^2 \tag{20}$$

since $cd = \pm 1$ has no effect on the statistics of each term separately, and the sum of L i.i.d. standard normal samples has a variance equal to L. The last term of (19) is the same as the noise-only scenario described in (14), and is therefore also normally distributed with zero mean and variance σ_w^4 as in (15). By assuming that the terms of (19) are independent, $R_{yy}^{(m)}(k)$ can be described as a normally distributed RV with mean $\mu_R^{(m)}$ equal to the first term of (19), and variance given by

$$\sigma_R^2 = 2\ \sigma_x^2\sigma_w^2 + \sigma_w^4 \tag{21}$$

which is the sum of the variances of the three random terms in (19). The independence assumption is based on the fact that $k \neq 0$, the noise samples are i.i.d., and the spreading chips and data bits are independent. (Independence can further be ensured using a dual-channel receiver structure as in [18].)

By substituting (19) into (6), $\rho(k)$ becomes the sum of squares of M nonzero-mean Gaussian RVs. The distribution of $\rho(k)$ can therefore be determined using the non-central Chi-squared distribution $\mathcal{X}_M'^2$ [17]. By normalising the variance of $\rho(k)$ it can then be shown that

$$\frac{M}{\sigma_R^2}\rho(k) \sim \mathcal{X}_M'^2 \tag{22}$$

with non-centrality parameter

$$p_{nc} = \frac{1}{\sigma_R^2}\sum_{m=1}^{M}\left[\mu_R^{(m)}\right]^2 \tag{23}$$

since $R_{yy}^{(m)}(k)$ must be divided by σ_R to normalise the variance.

a) Peak value:
When the spreading sequences align, the first term of (19) equals (8), and the mean value $\mu_R^{(m)}$ therefore equals (9). Using (9) as the mean value in (23), the non-centrality parameter can then be determined as

$$p_{nc} = \frac{\sigma_x^4 LM}{\sigma_R^2} \tag{24}$$

It can be confirmed in simulation that the peak value $\rho(k = N)$ scaled according to (22) will have a non-central Chi-squared distribution with non-centrality parameter given in (24).

b) Sidelobe values:
When the spreading sequences are misaligned, the first term of (19) equals (11), and the mean value $\mu_R^{(m)}$ therefore equals (12). Using (12) and (23), the non-centrality parameter can therefore be calculated as

$$p_{nc} = \frac{\sigma_x^4 M}{\sigma_R^2 L} \tag{25}$$

It can also be confirmed in simulation that the sidelobe values $\rho(k \neq N)$ scaled according to (22) will have a non-central Chi-squared distribution with non-centrality parameter given in (25).

D. Estimation performance bound

Estimation algorithm 1 takes the index k of the maximum value of the mean-square correlation sequence $\rho(k)$ as the estimated sequence length N_{est}. The sequence length will therefore be estimated correctly if the peak of $\rho(k)$ is located at $k = N$. The estimation performance bound will be expressed in terms of the probability of correct estimation P_{ce}, which is the probability that the value $\rho(k)$ located at $k = N$ exceeds all other values located at $k \neq N$, defined as

$$P_{\text{ce}} = p\left\{\rho(k = N) > \rho(k \neq N)\right\} \tag{26}$$

with $k = 1, 2, \ldots, K$ chosen such that a single distinct peak will be present within $\rho(k)$, assuming the SNR is sufficiently high as in Fig. 3(b). By defining the RVs $\rho_{\text{peak}} = \rho(k = N)$ and the largest sidelobe contender $\rho_{\max} = \max[\rho(k \neq N)]$, the performance bound can further be developed from (26) as

$$\begin{aligned} P_{\text{ce}} &= p\left(\rho_{\text{peak}} - \rho_{\max} > 0\right) \\ &= \int_0^{\infty} f_{\text{diff}}(z)\ dz \end{aligned} \tag{27}$$

with $f_{\text{diff}}(z)$ the probability density function (PDF) of the RV difference $\rho_{\text{peak}} - \rho_{\max}$, which can be calculated using [16]

$$f_{\text{diff}}(z) = \int_{-\infty}^{\infty} f_{\text{peak}}(z+v)\ f_{\max}(v)\ dv \tag{28}$$

which is simply the convolution between $f_{\text{peak}}(z)$ and $f_{\max}(z)$, respectively the PDFs of ρ_{peak} and $\rho_{\max}$. $f_{\text{peak}}(z)$ is the non-central Chi-squared PDF with non-centrality parameter given in (24), and $f_{\max}(z)$ is the PDF of the maximum of the $K-1$ sidelobe values, where each one has a non-central Chi-squared PDF with non-centrality parameter given in (25). $f_{\max}(z)$ can therefore be expressed as [16]

$$f_{\max}(z) = (K-1) f_{\text{side}}(z) \left[F_{\text{side}}(z)\right]^{K-2} \tag{29}$$

with $f_{\text{side}}(z)$ and $F_{\text{side}}(z)$ respectively the PDF and cumulative distribution function (CDF) of each of the i.i.d. sidelobe values. By evaluating (27) to (29) numerically, the performance bound in terms of P_{ce} over a range of SNR values (with L and M fixed) can be obtained as is done in Section V.

E. Choice of parameter values

It is important to note that the bound derived in Section III-D is the optimal estimation performance for technique 1. The bound is a function of the parameter values K (or range of k), L, M and the SNR, under the assumptions that the segments and sequences align as in Fig. 4(b), and that a single correlation peak is present as in Fig. 3(b).

The actual estimation performance depends on the choice or assumptions made regarding these parameter values. The range of k constrains the estimated sequence length N_{est}, and technique 1 can therefore only provide the correct answer as long as $k = N$ is considered within the range of k. The positions of segments within the intercepted signal and the value of L will also influence the performance as described in Section III-A (see Fig. 4). The number of segments M required to estimate N depends on the SNR, although the number of segments available may be less than required, depending on the number of samples (containing the DSSS signal) intercepted. It can be shown that a lower SNR value will require more segments to maintain a given P_{ce} value, as more segments will be required to reduce or average out the noise.

Although the estimation technique presented here is blind, parameter values for K, L and M must be chosen correctly in order to determine N. The ranges of k and L may be set up according to known or expected DSSS sequence lengths or an exhaustive search may be required to find an autocorrelation peak. Although real-time application of the algorithm is possible in high-SNR scenarios, the typical low-SNR scenario considered in this paper will necessitate off-line analysis on a high-performance computing (HPC) platform as large values of M (and large ranges of k and L) would be required to perform estimation.

IV. Estimation technique 2: Eigen Analysis

Eigenvalues are used in several signal analysis techniques, including signal detection and parameter estimation. PCA [19] and singular value decomposition (SVD) [20] are two such related approaches where the principal components (dominant eigenvectors) or singular values (square roots of eigenvalues) are extracted from a matrix constructed from the intercepted signal. An example PCA technique to estimate spreading sequences by concatenating the first two eigenvectors of the covariance matrix of the intercepted signal is presented in [21]. Several SVD methods used to estimate the parameters of sinusoids in noise are available in the literature. Examples include estimation of signal parameters via rotational invariance techniques (ESPRIT) [22] and matrix pencil algorithms [23], where generalised eigenvalues of matrix pencils are extracted to estimate the parameters of interest [24].

More recently, eigenvalue techniques have been suggested to perform spectrum sensing in cognitive radio applications [25]. The presence of a primary user can be detected by using test statistics based on eigenvalues of a fusion matrix constructed from signal samples collected cooperatively from distributed sensors [26]. A similar DSSS detection technique that uses the largest eigenvalue of the covariance matrix of the intercepted signal as test statistic is presented in [8].

In this section we wish to show that the detection technique described in [8] can be adapted to determine the sequence length of a hidden DSSS transmission. Subsequently, the portion of the technique presented in [8] which is required to develop the sequence estimation algorithm is reviewed, and the estimation technique itself is then presented.

A. Largest eigenvalue sequence

The detection technique of [8] consists of two stages. During the first stage, the baseband intercepted signal of (1) is divided into non-overlapping segments containing D samples each, and the segments are then stacked to form the $D \times D$ detection matrix given by

$$\boldsymbol{Y} = \sigma_x \boldsymbol{X} + \sigma_w \boldsymbol{W} \tag{30}$$

with $\boldsymbol{X}$ the data matrix (containing the spreaded data) and $\boldsymbol{W}$ the AWGN matrix with i.i.d. elements.

During the second stage, the largest eigenvalue $\lambda_{Y,1}$ of the sample covariance matrix (SCM) of $\boldsymbol{Y}$, denoted as [19]

$$\boldsymbol{R}(\boldsymbol{Y}) = \frac{\boldsymbol{Y}^T \boldsymbol{Y}}{D} \tag{31}$$

is calculated. A sequence of largest eigenvalues of $\boldsymbol{R}(\boldsymbol{Y})$ is then formed by cyclically shifting the elements of $\boldsymbol{Y}$ to the left and upwards, such that the first element in each row moves to the last element of the row above it. The top left element of $\boldsymbol{Y}$ is removed, and the lower right element takes on a new sample value. For each cyclic or time shift τ of $\boldsymbol{Y}$, the largest eigenvalue is calculated, to form a sequence $\lambda_{Y,1}(\tau)$.

Fig. 5 shows the largest eigenvalue sequences formed when the Barker-11 code is considered for different values of D, for the signal-only scenario ($\sigma_x = 1$ and $\sigma_w = 0$ in (30)). Clearly, when $D = N = 11$, the eigenvalue sequence exhibits a more regular pattern and has a larger mean (and variance) compared with the other values.

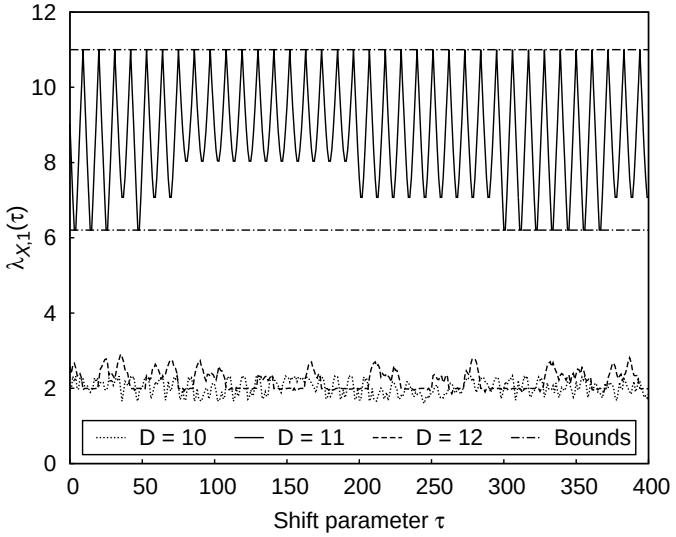

Fig. 5. Simulated largest eigenvalue sequences for the Barker-11 code for the signal-only scenario

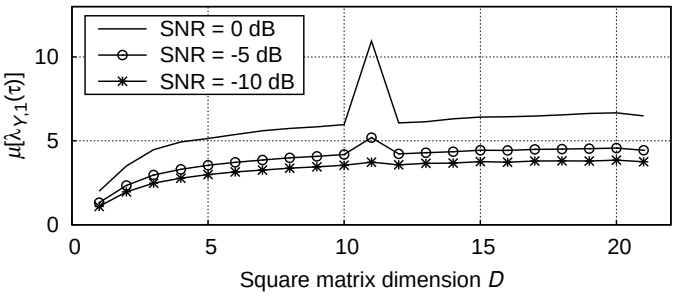

(a) Mean of largest eigenvalue sequence

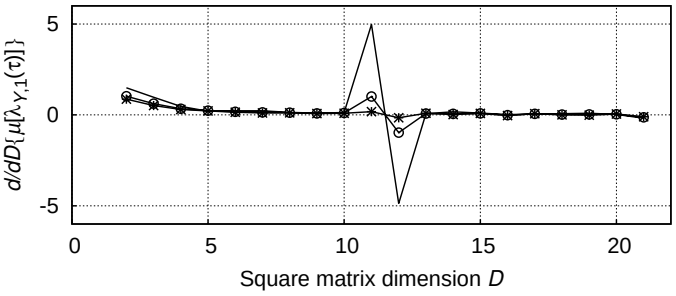

(b) Derivative of mean of largest eigenvalue sequence

Fig. 6. Simulated functions of the largest eigenvalue sequence over square matrix dimension D for SNR = $\{-10, -5, 0\}$ dB

B. Method of estimation

The sequence length can be determined by analysing the mean of the largest eigenvalue sequence $\lambda_{Y,1}(\tau)$ over a range of values of D as shown in Fig. 6(a). Similar to Fig. 3(a), the mean of $\lambda_{Y,1}(\tau)$ exhibits peak values at integer multiples of the spreading sequence length N.

The sequence length can therefore be determined by identifying the index of the peak in the graph shown in Fig. 6(a). Since the mean value increases along with D, the peak will be located at N only if the SNR is sufficiently high. The peak value can therefore be determined more reliably by identifying a decrease (or negative slope) within the mean value graph across the range of D. The technique presented here is therefore to estimate the sequence length using the minimum value of the derivative of the mean, shown in Fig. 6(b).

C. Mathematical analysis

Though it is possible to develop an analytic expression for the largest eigenvalue sequence, such an expression will be intractable since $\lambda_{X,1}$ depends on all the elements of $\boldsymbol{c}$ and $\boldsymbol{d}$ in (1). Instead, bounds on the variation of $\lambda_{Y,1}(\tau)$ will be developed in this section in order to describe its behaviour. The performance of the estimation technique will then be obtained through simulation which is presented in Section V.

1) Signal-only analysis: If the square matrix dimension D matches the spreading code length N, and $\sigma_w = 0$ in (30), the SCM

$$\boldsymbol{R}(\boldsymbol{Y}) = \sigma_x^2 \boldsymbol{R}(\boldsymbol{X}) \tag{32}$$

from (31) has a maximum rank of two, such that its eigenvalues are the roots of a quadratic polynomial, which can be expressed in the form [8]

$$\lambda_X = \frac{N^2 \pm \sqrt{\Delta}}{2N} \sigma_x^2 \tag{33}$$

since the spreading code and data bits have values ± 1. Also note that both eigenvalues will be nonnegative, as the SCM $\boldsymbol{R}(\cdot)$ is positive semidefinite [17]. As illustrated in Fig. 5 for $D = N$, $\lambda_{X,1}(\tau)$ exhibits a pattern with period N as $\boldsymbol{X}$ is cyclically shifted. By considering all possible combinations of code and data values for any cyclic shift of $\boldsymbol{X}$, it can be shown that the discriminant in (33) has ranges

$$\Delta \in \begin{cases} \left[0, N^4\right] & (N \text{ even}) \\ \left[2N^2 - 1, N^4\right] & (N \text{ odd}) \end{cases} \tag{34}$$

and the largest eigenvalue sequence is therefore bounded according to

$$\lambda_{X,1} \in \begin{cases} \left[\frac{N}{2}, N\right] \sigma_x^2 & (N \text{ even}) \\ \left[\frac{N^2 + \sqrt{2N^2 - 1}}{2N}, N\right] \sigma_x^2 & (N \text{ odd}) \end{cases} \tag{35}$$

which are the bounds shown (for N odd) in Fig. 5.

2) Noise-only analysis: If $\sigma_x = 0$ in (30) such that $\boldsymbol{Y} = \sigma_w \boldsymbol{W}$, the SCM

$$\boldsymbol{R}(\boldsymbol{Y}) = \sigma_w^2 \boldsymbol{R}(\boldsymbol{W}) \tag{36}$$

from (31) is a Wishart matrix [27]. The distribution of the largest eigenvalue of a Wishart matrix can be described using the Tracy-Widom (TW) law [28], which can be approximated using the Gamma distribution [29]. Using functions of distributions [16], the distribution of the largest eigenvalue $\lambda_{W,1}$ of (36) can be expressed using the Gamma PDF, given by [29]

$$\gamma(z) = \frac{(z - z_0)^{\alpha - 1}}{\theta^\alpha \Gamma(\alpha)} \exp\left[\frac{-(z - z_0)}{\theta}\right] \tag{37}$$

with $\Gamma(\cdot)$ the Gamma function, z_0 the location parameter, α the shape, and θ the scale, respectively given by

$$z_0 = \frac{\sigma_w^2\,(\mu_c - 9.8209\;\sigma_c)}{D}$$
$$\alpha = 46.5651$$
$$\theta = \frac{0.1850\;\sigma_w^2\;\sigma_c}{D}$$

with centre and scaling parameters [27]

$$\mu_c = \left(\sqrt{D-1} + \sqrt{D}\right)^2$$
$$\sigma_c = \sqrt{\mu_c}\left(\frac{1}{\sqrt{D-1}} + \frac{1}{\sqrt{D}}\right)^{\frac{1}{3}}$$

Furthermore, the support region of (37) can be expressed as [29]

$$z \in [z_0, z_0 + 2\alpha\theta] \tag{38}$$

3) Signal-and-noise analysis: When both $\sigma_x > 0$ and $\sigma_w > 0$ in (30), the SCM of (31) can be written as

$$\boldsymbol{R}(\boldsymbol{Y}) = \sigma_x^2\boldsymbol{R}(\boldsymbol{X}) + \sigma_w^2\boldsymbol{R}(\boldsymbol{W}) + \boldsymbol{E} \tag{39}$$

with the cross-term or error matrix

$$\boldsymbol{E} = \frac{\sigma_x\sigma_w}{D}\left[\boldsymbol{X}^T\boldsymbol{W} + \boldsymbol{W}^T\boldsymbol{X}\right] \tag{40}$$

which is zero under the assumption that the signal and noise are uncorrelated. Under this assumption, $\boldsymbol{R}(\boldsymbol{Y})$ is a linear function of $\boldsymbol{R}(\boldsymbol{X})$ and $\boldsymbol{R}(\boldsymbol{W})$ as indicated by (39), although the eigenvalues of $\boldsymbol{R}(\boldsymbol{Y})$ are nonlinear functions of the eigenvalues of $\boldsymbol{R}(\boldsymbol{X})$ and $\boldsymbol{R}(\boldsymbol{W})$ [30]. According to the Weyl inequalities [30]–[32], the largest eigenvalue of $\boldsymbol{R}(\boldsymbol{Y})$ is however bounded according to

$$\lambda_{\min} \leq \lambda_{Y,1} \leq \lambda_{\max} \tag{41}$$

with the upper and lower bounds given by [8]

$$\lambda_{\max} = [\lambda_{X,1}]_{\max} + [\lambda_{W,1}]_{\max} \tag{42}$$
$$\lambda_{\min} = \max\left\{[\lambda_{X,1}]_{\min}, [\lambda_{W,1}]_{\min}\right\} \tag{43}$$

Note that both $[\lambda_{X,1}]_{\min}$ and $[\lambda_{W,1}]_{\min}$ are less than or equal to $\lambda_{Y,1}$, though the tightest lower bound is obtained by taking the maximum of the two. The upper bound can be written from (42) as [29]

$$\lambda_{\max} = N\sigma_x^2 + z_0 + 2\alpha\theta \tag{44}$$

using the upper bounds given in (35) and (38). The lower bound can similarly be obtained from (43) using the lower bounds of (35) and (38). For N odd, the lower bound can therefore be expressed as

$$\lambda_{\min} = \max\left\{\frac{N^2 + \sqrt{2N^2-1}}{2N}\sigma_x^2, z_0\right\} \tag{45}$$

from which it can easily be shown that $\lambda_{\min} = z_0$ for small SNR values.

A simulated example of the largest eigenvalue sequence for $\sigma_x = \sigma_w = 1$ (SNR of 0 dB) is shown in Fig. 7 for the Barker-11 code for different values of D similar to Fig. 5. The eigenvalue bounds given in (44) and (45), and the measured mean value λ_μ of $\lambda_{Y,1}(\tau)$ are also shown. When $D = N$, the mean λ_μ clearly exceeds the means of the eigenvalue sequences associated with $D \neq N$, which is also illustrated in Fig. 6(a).

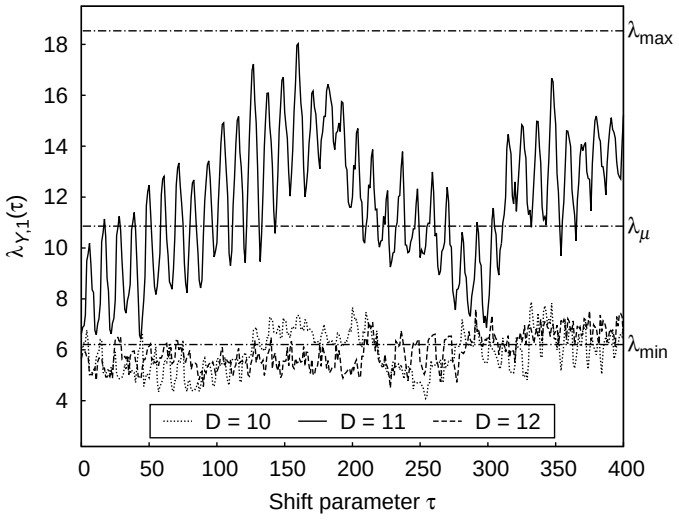

Fig. 7. Simulated largest eigenvalue sequences for the Barker-11 code for the signal-and-noise scenario

D. Choice of parameter values

The discussion of Section III-E is also relevant to technique 2. The range over which the matrix dimension D should be evaluated and the number of matrices (maximum time shift τ) to be considered to calculate the average eigenvalue must be chosen, similar to the suggestions made for the parameters of technique 1. As the calculation of eigenvalues are computationally expensive [8], technique 2 will also typically require off-line analysis.

V. Simulation results

This section provides Monte Carlo simulation results obtained by implementing the communication and intercept models of Section II in software. The performance of the two estimation techniques presented in Sections III and IV were evaluated against a Barker code ($N = 11$) and m-sequence ($N = 63$) with generator polynomial $g(X) = X^6 + X + 1$. The output of each estimation technique is the estimated sequence length N_{est}, which is compared with the actual sequence length N in order to evaluate the performance of each estimation technique.

A. Probability of estimation

Fig. 8 shows the probability of estimation P_{est} obtained over a range of values for N_{est} when the Barker-11 code is considered. Fig. 8(a) shows the results obtained using technique 1 for segment lengths $L = \{5, 11\}$ and $\text{SNR} = \{-15, -12\}$ dB. The sidelobe values (for $N_{\text{est}} \neq N$) are shown to be uniformly distributed, while a peak is observable (depending on L and the SNR) at $N_{\text{est}} = N$. The peak value increases while the sidelobe values decrease, as the SNR increases. Furthermore,

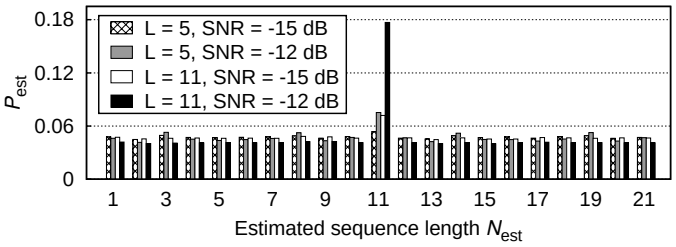

(a) Results obtained using technique 1

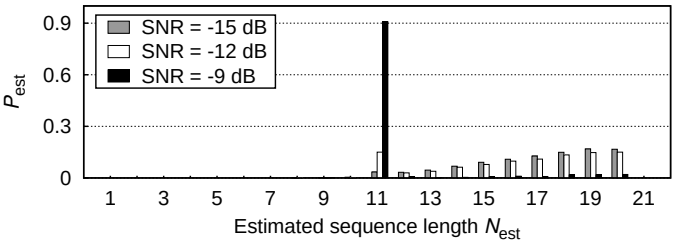

(b) Results obtained using technique 2

Fig. 8. Normalised histograms to indicate P_{est} for both estimation techniques against the Barker-11 code

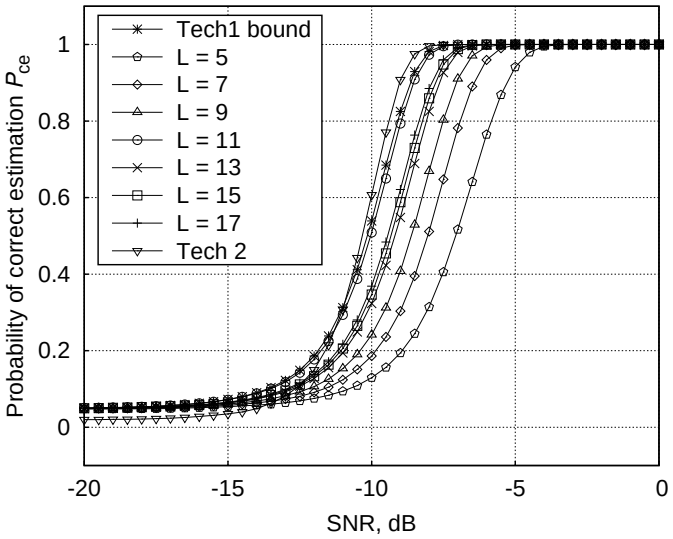

Fig. 9. Estimation performance of the two techniques against the Barker-11 code

the value at $N_{\text{est}} = N$ is the highest for $L = N$, provided that the SNR is sufficiently high.

Similarly, Fig. 8(b) shows the results obtained using technique 2 for different SNR values. The distribution of the sidelobe values can be explained from Fig. 6; the derivative of the mean of $\lambda_{Y,1}(\tau)$ is positive for small values of the square matrix dimension D, and decreases as D increases. The minimum value of the derivative will therefore typically (depending on the SNR) be located at $N_{\text{est}} \geq N$. As the SNR increases, the probability that $N_{\text{est}} = N$ will also increase.

B. Probability of correct estimation

As discussed in Section III-D, the performance of the estimation techniques can be evaluated in terms of the probability of correct estimation P_{ce}, which is the probability that N_{est} will equal N. Fig. 9 shows the simulated P_{ce} over a range of SNR values for the two estimation techniques against the Barker-11 code.

For technique 1, 10^5 runs of $M = 1000$ segments (of length L each) were simulated for each SNR point shown, with the maximum time shift $K = 2L - 1$. Different segment sizes L were considered, and when L matches $N = 11$, the best performance is obtained. When $L < N$, the performance degrades due to partial correlation of incomplete spreading sequences as explained in Section III-A. When $L > N$, the performance improves since some segments contain complete spreading codes, though the performance is still worse compared with $L = N$, since fragments of spreading codes within segments reduce the correlation peaks (also due to partial correlation). The theoretical bound for technique 1 given by (27) is also shown, which is nearly attained by the $L = 11$ curve. (The $L = 11$ curve does not match the theoretical curve *exactly* since L or N is not sufficiently long.)

For technique 2, the mean of the largest eigenvalue sequence λ_μ was calculated by shifting 1000 bits through the detection matrix $\boldsymbol{Y}$ as explained in Section IV. The same data sequence was used to calculate λ_μ for a single simulation run, during which the range of matrix dimensions $D = 1, \ldots, 2N-1$ were evaluated for each SNR point. A total of 10^4 simulation runs was completed per SNR value. Fig. 9 indicates that technique 2 outperforms the best possible performance of technique 1 for SNR values exceeding approximately -11 dB. When the segment size of technique 1 is chosen as $L = 5$, technique 2 outperforms technique 1 by up to 4 dB.

Similar to Fig. 9, the simulated P_{ce} performances of the two estimation techniques against the length-63 m-sequence are shown in Fig. 10. The theoretical performance bound for technique 1 predicted in (27) is approached for $L = N$, and worse performances are shown for both $L < N$ and $L > N$ as in Fig. 9. Furthermore, technique 2 exceeds the best possible performance of technique 1 by approximately 4 dB. By comparing Figs. 9 and 10, it is clear that the estimation performance improves for a larger value of N.

Figs. 9 and 10 also indicate that both techniques 1 and 2 will be able to correctly estimate the sequence lengths (with $P_{\text{ce}} = 1$) of DSSS transmissions at the SNR levels given in terms of the maximum tolerable BER and channel requirements described in Section II.

VI. Conclusion

Two novel techniques based on autocorrelation and PCA were presented to blindly estimate the sequence length N of an intercepted DSSS transmission hidden within noise. Mathematical analyses and results of a simulation study for each technique were given.

The autocorrelation technique computes the mean-square correlation between segments of the intercepted signal and takes the index value of the first peak as the sequence length. The performance of this technique depends on the choice of the segment length L, with best performance if $L = N$. Furthermore, the range of k over which the correlation peak

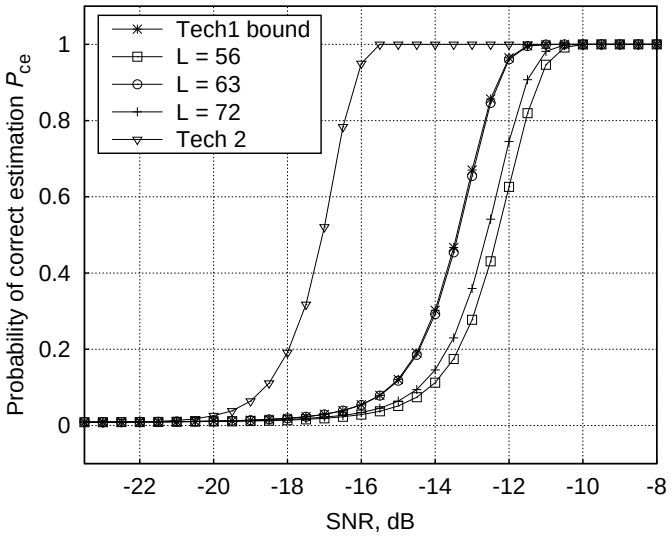

Fig. 10. Estimation performance of the two techniques against the length-63 m-sequence

is searched must include $k = N$ and the number of segments M must be sufficient to suppress the noise. This technique is similar to the correlation spike spacing estimation algorithm suggested in [11], and was used to establish a reference performance in terms of probability of correct estimation P_{ce} over SNR.

The eigen-analysis technique computes the mean value λ_μ of the largest eigenvalue sequence of the intercepted signal for a range of square data matrix dimensions D. It was shown in this paper that λ_μ is much larger when D equals the spreading sequence length N. The sequence length can therefore be determined as the value of D at which λ_μ versus D has a peak value. The eigen-analysis technique, adapted from the detection technique of [8], was also shown to have superior estimation performance compared with the reference autocorrelation technique.

VII. Future work

In this paper it was assumed that the signal of interest was detected first such that the estimation algorithm was applied to a signal that is surely present within noise. However, it cannot always be ascertained that the signal of interest *is* present before attempting to perform estimation. In certain applications, detection and estimation can be formulated as a single problem which can provide improved results [33]. The estimation techniques presented in this paper can be adapted to function as detection algorithms by using the estimated parameters as detection test statistics. A confidence level that the sequence length is estimated correctly can also be established by evaluating the consistency of the estimated value.

Furthermore, only spreading codes with noise-like autocorrelation characteristics, including Barker codes and m-sequences, were considered in this paper. How to blindly estimate the sequence length of orthogonal codes, such as Walsh codes which have multiple sidelobe correlation peaks, remains an open question.

VIII. Acknowledgement

This work was supported by the Armaments Corporation of South Africa (Armscor) under contract no. KT521909. The authors would like to thank the anonymous reviewers for their valuable inputs.

References

1 Proakis, J.G., Salehi, M.: 'Digital communications' (McGraw-Hill, Boston, MA, USA, 2007, 5th edn.)
2 Kay, S.M.: 'Fundamentals of statistical signal processing: Estimation theory' (Prentice Hall, Upper Saddle River, NJ, USA, 1993, vol. 1)
3 Middleton, D.: 'Non-Gaussian statistical communication theory' (Wiley-IEEE Press, Hoboken, NJ, USA, 2012)
4 Torrieri, D.J.: 'Principles of spread-spectrum communication systems' (Springer, New York, NY, USA, 2011, 2nd edn.)
5 Zhan, Y., Cao, Z., Lu, J.: 'Spread-spectrum sequence estimation for DSSS signal in non-cooperative communication systems', *IEE Proc. Commun.*, 2005, **152**, (4), pp. 476–480
6 Tsatsanis, M.K., Giannakis, G.B.: 'Blind estimation of direct sequence spread spectrum signals in multipath', *IEEE Trans. Signal Process.*, 1997, **45**, (5), pp. 1241–1252
7 Dominique, F., Reed, J.: 'Simple PN code sequence estimation and synchronisation technique using the constrained Hebbian rule', *IEE Electron. Lett.*, 1997, **33**, (1), pp. 37–38
8 Vlok, J.D., Olivier, J.C.: 'Non-cooperative detection of weak spread-spectrum signals in additive white Gaussian noise', *IET Commun.*, 2012, **6**, (16), pp. 2513–2524
9 Gardner, W.A., Spooner, C.M.: 'Signal interception: performance advantages of cyclic-feature detectors', *IEEE Trans. Commun.*, 1992, **40**, (1), pp. 149–159
10 Adams, E.R., Gouda, M., Hill, P.C.J.: 'Statistical techniques for blind detection & discrimination of m-sequence codes in DS/SS systems'. Proc. IEEE-ISSSTA, Sun City, South Africa, Sep. 1998, vol. 3, pp. 853–857
11 Burel, G.: 'Detection of spread spectrum transmissions using fluctuations of correlation estimators'. Proc. IEEE-ISPACS, Honolulu, Hawaii, USA, Nov. 2000
12 Burel, G., Bouder, C., Berder, O.: 'Detection of direct sequence spread spectrum transmissions without prior knowledge'. Proc. IEEE-GLOBECOM, San Antonio, TX, USA, Nov. 2001, vol. 1, pp. 236–239
13 Akyildiz, I.F., Levine, D.A., Joe, I.: 'A slotted CDMA protocol with BER scheduling for wireless multimedia networks', *IEEE/ACM Trans. Netw.*, 1999, **7**, (2), pp. 146–158
14 Sarwate, D.V., Pursley, M.B.: 'Crosscorrelation properties of pseudorandom and related sequences', *Proc. IEEE*, 1980, **68**, (5), pp. 593–619
15 Weisstein, E.W.: 'CRC concise encyclopedia of mathematics' (CRC Press, Boca Raton, Florida, USA, 2003, 2nd edn.)
16 Papoulis, A., Pillai, S.U.: 'Probability, random variables and stochastic processes' (McGraw-Hill, 2002, 4th edn.)
17 Kay, S.M.: 'Fundamentals of statistical signal processing: Detection theory' (Prentice Hall, Upper Saddle River, NJ, USA, 2011, vol. 2)
18 Houghton, A.W., Reeve, C.D.: 'Detection of spread-spectrum signals using the time-domain filtered cross spectral density', *IEE Proc. Radar Sonar Navig.*, 1995, **142**, (6), pp. 286–292
19 Bejan, A.: 'Largest eigenvalues and sample covariance matrices'. MSc dissertation, Department of Statistics, University of Warwick, UK, 2005
20 Golub, G.H., Van Loan, C.F.: 'Matrix computations' (John Hopkins University Press, Baltimore, MD, USA, 1996, 3rd edn.)
21 Bouder, C., Azou, S., Burel, G.: 'Performance analysis of a spreading sequence estimator for spread spectrum transmissions', *Elsevier J. Frankl. Inst.*, 2004, **341**, (7), pp. 595–614
22 Roy, R., Kailath, T.: 'ESPRIT–Estimation of signal parameters via rotational invariance techniques', *IEEE Trans. Acoust., Speech, Signal Process.*, 1989, **37**, (7), pp. 984–995
23 Hua, Y., Sarkar, T.K.: 'Matrix pencil method for estimating parameters of exponentially damped/undamped sinusoids in noise', *IEEE Trans. Acoust., Speech, Signal Process.*, 1990, **38**, (5), pp. 814–824
24 Hua, Y., Sarkar, T.K.: 'On SVD for estimating generalized eigenvalues of singular matrix pencil in noise', *IEEE Trans. Signal Process.*, 1991, **39**, (4), pp. 892–900

25 Zeng, Y., Liang, Y.C.: 'Eigenvalue-based spectrum sensing algorithms for cognitive radio', *IEEE Trans. Commun.*, 2009, **57**, (6), pp. 1784–1793
26 Wei, L., Tirkkonen, O.: 'Analysis of scaled largest eigenvalue based detection for spectrum sensing'. Proc. IEEE ICC, Kyoto, Japan, Jun. 2011, pp. 1–5
27 Johnstone, I.M.: 'On the distribution of the largest eigenvalue in principal component analysis', *Ann. Stat.*, 2001, **29**, (2), pp. 295–327
28 Tracy, C., Widom, H.: 'The distribution of the largest eigenvalue in the Gaussian ensembles', in Van Diejen, J.F., Vinet, L. (Eds.): 'Calogero-Moser-Sutherland models: CRM series in mathematical physics 4' (Springer-Verlag, 2000), pp. 461–472
29 Vlok, J.D., Olivier, J.C.: 'Analytic approximation to the largest eigenvalue distribution of a white Wishart matrix', *IET Commun.*, 2012, **6**, (12), pp. 1804–1811
30 Everson, R., Roberts, S.: 'Inferring the eigenvalues of covariance matrices from limited, noisy data', *IEEE Trans. Signal Process.*, 2000, **48**, (7), pp. 2083–2091
31 Horn, R.A., Johnson, C.R.: 'Matrix analysis' (Cambridge University Press, Cambridge, UK, 2012, 2nd edn.)
32 Tao, T.: 'Topics in random matrix theory (Graduate studies in mathematics)' (American Mathematical Society, Rhode Island, USA, 2012)
33 Moustakides, G.V., Jajamovich, G.H., Tajer, A., Wang, X.: 'Joint detection and estimation: Optimum tests and applications', *IEEE Trans. Inf. Theory*, 2012, **58**, (7), pp. 4215–4229